Chapter 9

Electronic states in circular and ellipsoidally deformed quantum dots

***S Tarucha*[1,2], *D G Austing*[2], *S Sasaki*[2], *L P Kouwenhoven*[3], *S M Reimann*[4], *M Koskinen*[4] *and M Manninen*[4]**
[1] ***Department of Physics, University of Tokyo, 7-3-1, Hongo, Bunkyo-ku, Tokyo, 113-0033, Japan***
[2] ***NTT Basic Research Laboratories, 3-1, Morinosato, Wakamiya, Atsugi-shi, Kanagawa 243-0198, Japan***
[3] ***Department of Applied Physics, Delft University of Technology, PO Box 5046, 2600 GA Delft, The Netherlands***
[4] ***University of Jyväskylä, Physics Department, PO Box 35, 40351, Jyväskylä, Finland***

The electronic properties of circular and ellipsoidally deformed quantum dot single electron transistors are studied by measuring Coulomb oscillations of circular and rectangular mesas. The filling of the few electron ground states in circular mesa devices at zero magnetic field gives rise to a pronounced shell structure characteristic of a two-dimensional harmonic confining potential with rotational symmetry, and is in accordance with Hund's first rule. These atomic-like features are readily disrupted in the rectangular mesa devices due to the lifting of the single-particle level degeneracies. Measurements with a magnetic field parallel to the current allow us to identify changes in the quantum numbers labelling the electronic states which are induced by the deformation. In particular, the transition from a spin-triplet in a circular dot to a spin-singlet in elliptical dots for the four-electron ground state at zero-magnetic field is investigated. The spin-singlet in the rectangular mesa is clearly identified independently from the measurement of the Zeeman effect. These observations are in good agreement with model calculations based on spin-density functional theory, and a single-particle picture is also very useful. Even for a small deformation, breaking the

circular symmetry significantly modifies the shell structure and changes the total spin of a state. Finally, we argue that the magnetic field dependence for the rectangular mesa devices suggests that the anisotropy of an elliptical dot may be much higher than that suggested by the geometry of the device mesa in which the dot is located.

9.1 Introduction

Recent advances in epitaxial growth and processing technology have enabled us to fabricate semiconductor nanostructures whose dimensions are comparable to the de Broglie wavelength of electrons. Transport measurements of these nanostructures have revealed a variety of phenomena associated with the effects of quantum mechanical confinement [1]. Conductance quantization in one-dimensional quantum point contacts, and resonant tunnelling through quantum wires and quantum boxes are such examples. These properties directly reflect the quantization of energy. In addition, charge quantization is observed for electrons tunnelling through a small dot. This dot acts as an island for the electrons. When tunnelling occurs, the charge on the island suddenly changes by the quantized amount 'e'. This leads to a change in the electrostatic potential of the dot by a unit of energy called the 'charging energy', $E_{\mathrm{c}} = e^2/C$, where C is the typical capacitance of the island. The one-by-one change in the number of electrons on the island, N, gives rise to oscillations in the tunnelling conductance (Coulomb oscillations) when the gate voltage is swept. These oscillations are usually periodic when the number of electrons is 'large'. However, in a small dot holding just a few electrons, the charging energy can no longer be parametrized with a constant capacitance, and the Coulomb oscillations are significantly modified by electron–electron interactions, and quantum confinement effects. Thus, the *addition energy* needed to put an extra electron on the dot becomes strongly dependent on the number of electrons on the dot. Such a system can be regarded as an artificial atom [2].

The energy spectrum of a quantum dot has been extensively studied for small semiconductor dots, using so-called single electron transistors (SETs) with many different geometries and configurations. This is particularly true for SETs with a planar geometry defined in a two-dimensional electron gas by surface Schottky gates. The lateral constrictions forming the dot, the tunnel junctions between the dot and the reservoirs, and the plunger gate used to tune the electrostatic potential of the dot are all made by the Schottky gates. This enables a wide variation of device geometry, and a large freedom of gate operation for tuning the transmission probability of the tunnel junctions as well as the electron number in the dot. However, there are a number of limitations. For example, the geometry of the dot is not so well defined since the actual confining potential imposed by the Schottky gates can be significantly different from the gate geometry. In addition, it is almost impossible to fabricate a dot containing just a few electrons. In contrast, due to

the presence of heterostructure tunnel barriers and vertical side walls, the dot in a vertical quantum dot SET can have both good shape and high symmetry. Such a vertical SET allows N to be precisely tuned, *starting from zero*. The fabrication technology has only recently been developed [3, 4]. Transport measurement on vertical SETs reveals atom-like properties such as a two-dimensional (2D) 'shell structure' and filling in accordance with Hund's first rule. The high symmetry of the vertical circular dot leads to maximal level degeneracy of the 2D single-particle states for parabolic lateral confinement. At 0 T, consecutive filling of each set of degenerate states is directly responsible for the characteristic shell structure, and Hund's first rule accounts for the parallel filling of electrons amongst a half-filled shell of degenerate states. In this paper we first review the atom-like properties observed for the circular dot. Then, we discuss the effect of anisotropy in the lateral confinement on the shell structure and the spin states. Breaking the circular symmetry by deforming the lateral confining potential lifts the degeneracies present in the circular dot, and 'destroys' the distinctive shell structure for the circle, and modifies other atomic-like properties [5, 6]. In the experiment, we use rectangular dots to study the effect of anisotropy in the lateral confinement, and compare results to model calculations based on spin-density functional theory. In addition, we measure the Zeeman effect to identify the spin states in the rectangular dots.

9.2 Experimental details

We use a double barrier structure (DBS) to fabricate vertical quantum dots with a high degree of cylindrical symmetry in the lateral confinement, and with an asymmetry in the lateral confinement. The DBS consists of an undoped 13 nm $In_{0.05}Ga_{0.95}As$ well and two undoped $Al_{0.22}Ga_{0.78}As$ barriers of thickness 9.0 and 7.5 nm, and this is processed to form one circular mesa with a nominal top contact diameter, D, of 0.5 μm (W), and three rectangular mesas with top contact area (L$\times$S)$0.55\times0.4\,\mu m^2$ (X), $0.65\times0.45\,\mu m^2$ (Y), and $0.6\times0.4\,\mu m^2$ (Z). L (S) is the nominal dimension of longest (shortest) side of the top contact [3, 4]. Figure 9.1 shows a schematic diagram of the circular mesa device. Above and below the DBS there is an n-doped GaAs contact (source and drain), and the circular dot is located between the two heterostructure barriers. A single Schottky gate is placed on the side of the mesa, wrapping round the dot. Figure 9.2 shows typical scanning electron micrographs of a circular mesa, and a rectangular mesa taken immediately after the deposition of the gate metal. For the rectangular mesas, a simple way to classify them is to define a geometric parameter, β, to be the ratio L/S. For X, Y, and Z respectively, β is nominally 1.375, 1.44 and 1.5. Due to a slight undercut, the area of the mesas is a little less than that of the top contact. Figure 9.2 also shows schematically the slabs of semiconductor between the two tunnelling barriers, and the resulting dots bounded by the shaded depletion region.

The current, I, flowing vertically through the dot is measured as a function

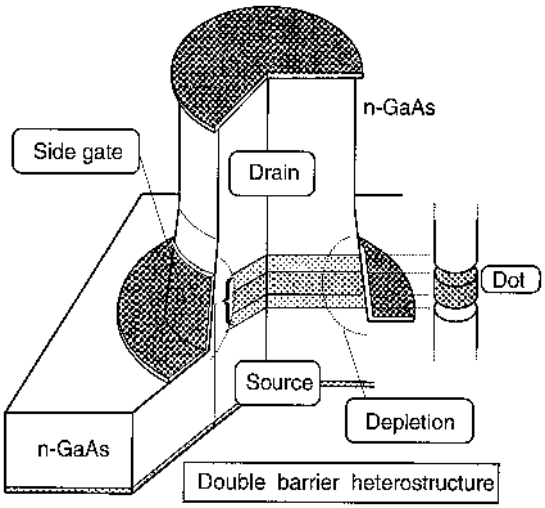

Figure 9.1. Schematic of the quantum dot in a vertical device.

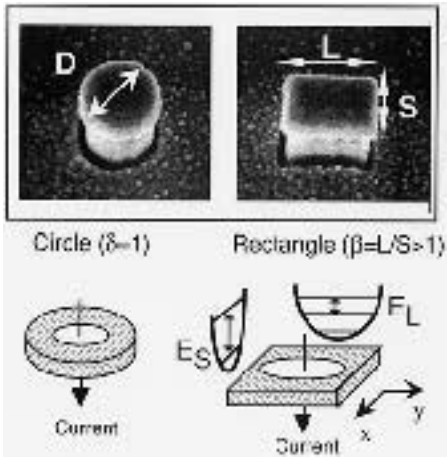

Figure 9.2. Scanning electron microscope (SEM) images showing submicrometre circular and rectangular mesas, and schematic diagrams of the resulting circular and elliptical shaped dots in the mesas.

of gate voltage, V_g, in response to a dc voltage, V_{sd}, applied between the contacts. For an arbitrarily small V_{sd}, the ground states (GSs) of an N-electron quantum dot can be investigated directly from monitoring the current. When no current flows (Coulomb blockade), the number of electrons in the dot, N, is well defined. On the other hand, when current flows the number of electrons can oscillate from N

to $N + 1$. Sweeping V_g, a series of sharp current peaks due to the charging of the dot (Coulomb oscillations) can be observed.

9.3 Electronic properties of circular quantum dots

9.3.1 Atom-like properties: shell structure and Hund's first rule

A good analogue to the three-dimensional shell in atoms [8] can be realized for an artificial atom with the shape of a circular disk. The disk-shaped quantum dots we can fabricate are formed in a laterally grated submicrometre DBS, and contain a tunable number of electrons starting from zero. If the lateral confinement has the form of a harmonic potential, the eigenenergy, $E_{n,\ell}$, for the lateral states are labelled using two orbital quantum numbers: the radial quantum number, $n(= 0, 1, 2, \ldots)$, and the angular momentum quantum number, $\ell(= 0, \pm 1, \pm 2, \ldots)$, and has the form:

$$E_{n,\ell} = (2n + |\ell| + 1)\hbar\omega_0, \tag{9.1}$$

where $\hbar\omega_0$ is the lateral confinement energy. Here, we neglect the Zeeman effect, so that each state is spin degenerate. $E_{n,\ell}$ eigenstates (n, ℓ) are systematically degenerate, so including spin degeneracy, states at 0 T in the first, second and third shells respectively are two-fold degenerate with energy $E_{0,0}$ (1s orbital), four-fold degenerate with energy $E_{0,1} = E_{0,-1}$ (2p orbitals), six-fold degenerate with energy $E_{0,2} = E_{0,-2}$ (3d orbitals) $= E_{1,0}$ (3s orbital). For non-interacting electrons these states are consecutively filled from the lowest, and complete filling of each set of degenerate states is attained for special electron numbers of $N = 2, 6, 12, 20, \ldots$. These are the 'magic numbers' that characterize the shell structure. For interacting electrons the degeneracy is lifted due to the Coulomb interactions. However, when the quantum mechanical confinement energy is comparable to, or greater than the interaction energy, the above shells are still consecutively filled from the lowest, so that we can define the same series of magic numbers as for the non-interacting case. In addition, for the filling of electrons in the same shell, parallel spins are favoured by Hund's first rule. This leads to another series of magic numbers of $N = 4, 9, 16, \ldots$, corresponding to the half filling of the second, third, fourth shells, respectively.

Figure 9.3 shows the current oscillations observed for a dot in a typical circular mesa device (W) [4]. A small bias of 0.15 mV is set for V_{sd}, so that only the GSs contribute to the current. The absolute values of N can be identified for each zero-current region between the peaks, starting from $N = 0$, because for $V_g < -1.6$ V no further current peaks are observed, i.e. the dot is empty. When N becomes smaller than 20, the oscillation period depends strongly on N. In contrast, Coulomb oscillations observed for large dots containing more than 100 electrons look very periodic [7]. The current peak to the left of a Coulomb blockade region with N trapped electrons thus measures the electrochemical potential, $\mu(N)$, of the N electron GS. The peak spacing labelled by 'N'

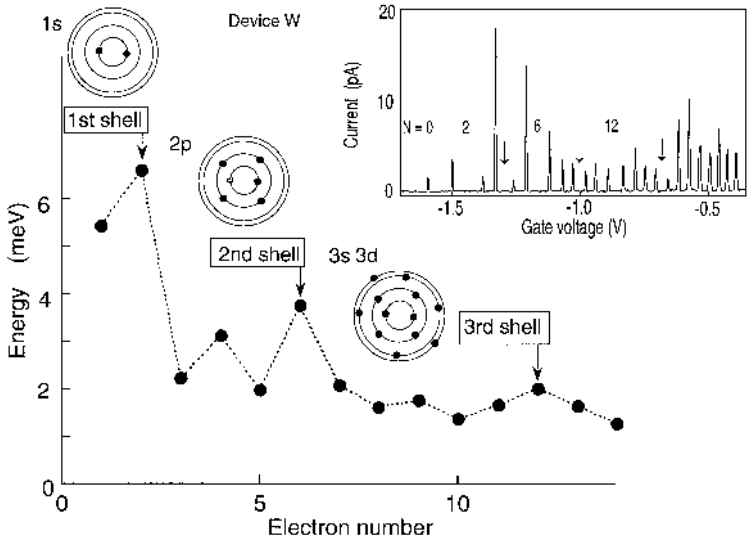

Figure 9.3. Change of the electrochemical potential, $\mu(N+1) - \mu(N+1)$, as a function of electron number, N [4]. Inset: Coulomb oscillations in current versus gate voltage at $B = 0$ T measured at 50 mK.

corresponds to the change of electrochemical potential, $\Delta_2(N) = \mu(N+1) - \mu(N)$. $\Delta_2(N)$, which can also be determined from measuring the widths of the so-called 'Coulomb diamonds', is plotted in figure 9.3. In correspondence with the pattern of spacings between the Coulomb oscillations, $\Delta_2(N)$ is unusually large for $N = 2$, 6 and 12, and is also relatively large for $N = 4$, 9 and 16 (see arrows in figure 9.3). The values of 2, 6 and 12 arise from the complete filling of the first, second and third shells, respectively, while those of 4, 9 and 16 are due, respectively, to the half filling of the second, third and fourth shells with parallel spins (Hund's first rule). The 2D shell structure is pictorially illustrated in figure 9.3.

9.3.2 Magnetic field dependence

In the presence of a magnetic field (B-field) parallel to the tunnelling current the electronic states are modified. This can be used to identify the quantum states in the dot. The eigenstates for a 2D harmonic potential are the Fock–Darwin (F–D) states [9]. The eigenenergies are expressed as:

$$E_{n,\ell} = -\frac{\ell}{2}\hbar\omega_c + \left(n + \frac{1}{2} + \frac{1}{2}|\ell|\right)\hbar\sqrt{4\omega_0^2 + \omega_c^2} \tag{9.2}$$

where $\hbar\omega_c = eB/m^*$ is the cyclotron frequency. Figure 9.4(a) shows $E_{n,\ell}$ versus B calculated for $\hbar\omega_0 = 3$ meV, which is a value deduced by a comparison with

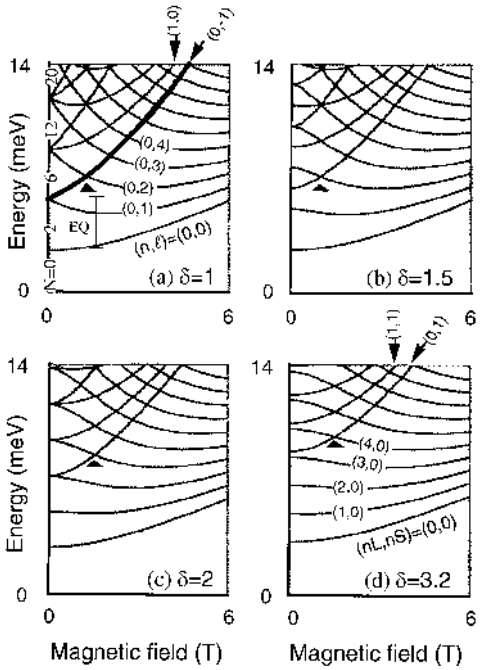

Figure 9.4. Calculated B-field dependence of the first ten single-particle energy levels for a circular dot with $\delta = 1$, and (a) for elliptical dots with $\delta = 1.5$, 2 and 3.2, (b)–(d) [5].

the experimental data [4]. Spin is neglected so each state is two-fold degenerate. The orbital degeneracy at $B = 0$ T is lifted on increasing B, reflecting the first term in equation (9.2). As B is increased further, new crossings can occur. The last crossings occur along the bold line in figure 9.4(a). Beyond this crossing the F–D states correspond to the lowest Landau level.

Figure 9.5(a) shows the B-field dependence of the position of the current oscillations (see also figure 9.3) [4]. We take into account the interaction energy as well as the F–D states to interpret the experimental data. The current peaks generally shift in pairs with B. This pairing is due to the lifting of spin degeneracy. So from the shift of the paired peaks on increasing B, we assign quantum numbers to the respective pairs. For example, up to about 1 T, the lowest, second lowest, and third lowest pairs seem to correspond to the filling of electrons in the F–D states $(n, \ell) = (0, 0)$, $(0, -1)$, and $(0, 1)$ with antiparallel spins, respectively. Also, at higher B-field, the 'wiggles' or anticrossings between pairs of peaks correspond to the crossings of F–D states. For example, the anticrossing at the * label corresponds to the crossing of the F–D states $(0, -1)$ and $(0, 2)$, and the anticrossing at the ** label corresponds to the crossing of the F–D states $(0, -1)$ and $(0, 3)$ (see figure 9.4(a)). However, from close inspection to the second and

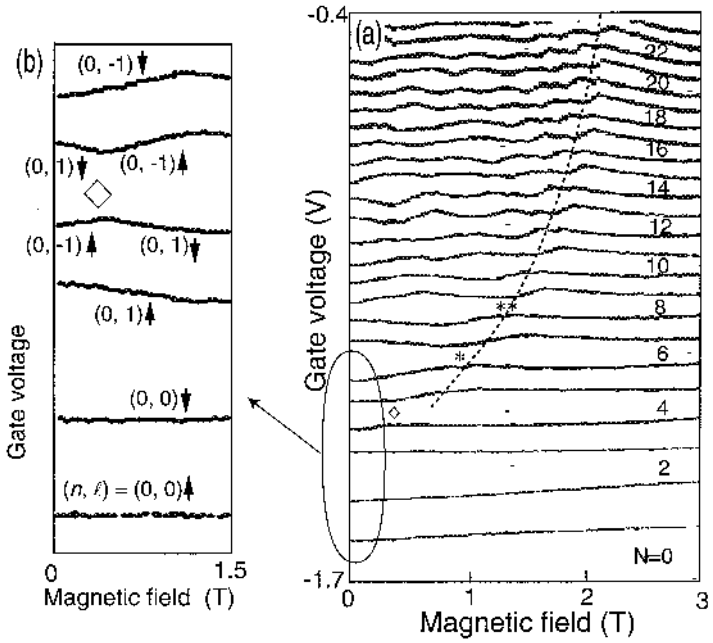

Figure 9.5. (*a*) B-field dependences of current peak positions measured for the device (W) whose Coulomb oscillations are shown in figure 9.3 [4]. (*b*) Magnified plot of the B-field dependences of the peak positions for the first six current peaks. The corresponding F–D states are indicated by (n, ℓ) quantum numbers, and by $\uparrow$ or $\downarrow$, where $\uparrow$ or $\downarrow$ is a state with an up-spin or a down-spin, respectively.

third lowest pairs of peaks in the vicinity of $B = 0$ T, we find that the pairing is further modified in line with Hund's first rule. The details will be discussed in the next section.

The last anticrossing of each pair of peaks appears along the dotted curve in figure 9.5(*a*), which corresponds to the bold curve in figure 9.4(*a*). This dotted curve actually identifies the regime of filling factor $\nu = 2$. For $\nu < 2$, we see various other transitions associated with B-field enhanced Coulomb interactions, such as spin flip transitions between $\nu = 2$ and 1 [10], a spin single-triplet transition for $N = 2$ at $\nu = 1$ [11, 12], and the formation of the so-called maximum density droplet for $N > 2$ at $\nu = 1$ [13].

9.3.3 Spin triplet for the four-electron ground state

The pairing in the current peaks as observed in figure 9.5(*a*) arises from the antiparallel spin filling of orbital states. This can be modified when interaction effects determining spin filling cannot be neglected. Figure 9.5(*b*) shows a

magnified plot for the first six peaks evolving with magnetic field close to 0 T. The pairing of the third peak with the fifth, and the fourth peak with the sixth from 0 to 0.4 T, as opposed to the usual pairing of the third peak with the fourth, and the fifth peak with the sixth for $B > 0.4$ T, is a consequence of Hund's first rule, i.e. the $N = 4$ state is a spin-triplet so two parallel-spin electrons fill the two originally degenerate states $(n, \ell) = (0, 1)$ and $(0, -1)$ in the half-filled second shell [4, 7]. For $B > 0.4$ T, the fifth and sixth peaks, as a pair, first move up, reflecting the value of angular momentum quantum number $\ell = -1$. The spins of the added electrons are shown pictorially in figure 9.5(*b*). To explain why Hund's first rule gives a spin-triplet, we can introduce energy, E_{EX}, to represent the reduction in energy due to exchange between same two spin electrons in the half-filled second shell (estimated to be about 0.7 meV for W [4, 7]). The $N = 4$ triplet-state is thus lower in energy than the $N = 4$ singlet-state at 0 T by E_{EX}, and as a consequence $\Delta_2(3, 5) < \Delta_2(4)$ by about $2E_{\mathrm{EX}}$. This effect persists as long as the splitting between states $(0, 1)$ and $(0, -1)$ is less than E_{EX}. At a critical B-field labelled by $\diamond$, this splitting exceeds E_{EX}, and the GS becomes a spin-singlet, i.e. there is a B-field induced triplet–singlet transition. This argument also implies that the first excited state (ES) is a spin-singlet for $B < 0.4$ T, whereas it is a spin-triplet for $B > 0.4$ T. We usually measure Coulomb oscillations to calculate only the GSs. To investigate the configurations of the GSs and ESs responsible for the triplet–singlet transition, we use an excitation spectroscopy technique [12].

Application of a bias voltage, V_{sd}, between the source and drain (typically a few meV) opens a 'transport window' between the Fermi energies for detecting both the N-electron GS and ESs in the dot (figure 9.6(*a*)). GSs and ESs lying within the transport window can contribute to current. If the gate voltage is made more positive, then the levels in the dot shift down in energy. When V_{sd} is smaller than the energy difference between the GS and lowest ES, only the GS contributes to the current, I, because the electron tunnelling into the ES is blocked. This is the usual case for measuring Coulomb oscillations, so we see just a series of current peaks as a function of gate voltage corresponding to the one-by-one change of electrons in the GSs of the dot (figure 9.3). When V_{sd} is sufficiently large, however, both the GSs and ESs can be within the transport window, and contribute to current. Electron tunnelling into the ESs can occur following the electron escape from a GS. I versus V_g therefore becomes a series of current 'stripes'. Changes in the current level inside each stripe are measured when the ESs enter the transport window. The boundaries of the current stripe identify when the GS enters or leaves the transport windows, so the stripe has a width in energy given by eV_{sd}.

Figure 9.6(*b*) shows the spectrum for the $N = 3$ and 4 GSs and ESs measured at $V_{\mathrm{sd}} = 1.6$ mV for a circular mesa device (not W). To emphasize variations in current we plot the derivative, $\mathrm{d}I/\mathrm{d}V_{\mathrm{g}}$, in the plane of V_{g} and B. The dark curves identify the GSs and ESs. The white long-dashed curves trace the GSs, and the first and second ESs are indicated by the white dotted- and dotted-dashed curves, respectively. The $N = 3$ GS and first ES follow the B-field dependence of F–D

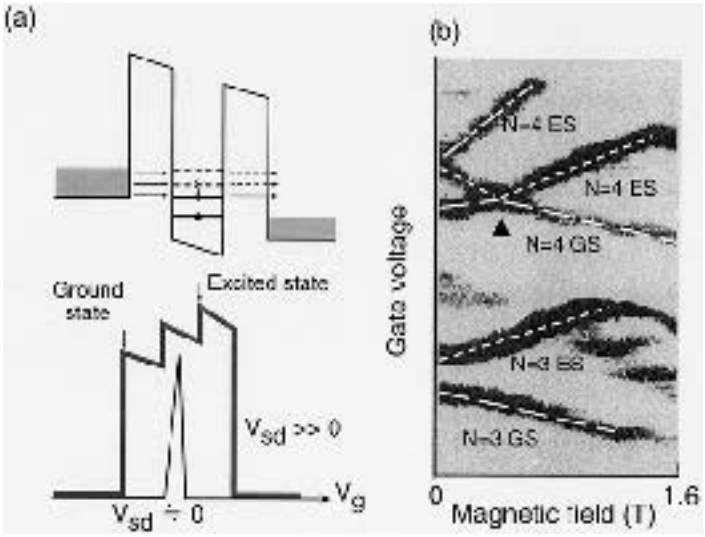

Figure 9.6. (*a*) Energy diagram and tunnelling current with a finite voltage is applied between the source and drain. (*b*) Derivative of the tunnelling current, $\mathrm{d}I/\mathrm{d}V_\mathrm{g}$, as a function of gate voltage and magnetic field measured for the circular mesa (not W) with $V_\mathrm{sd} = 1.6$ mV. Changes in the grey scale indicate changes in the current amplitude. The white long-dashed curves indicate the GSs, the first and second ESs are shown by the white dotted-, and chain curves.

states $(n, \ell) = (0, 1)$ and $(0, -1)$, respectively. On the other hand, the spectrum for $N = 4$ clearly shows the crossing of the F–D states $(0, 1)$ and $(0, -1)$ at 0.4 T, which causes the singlet–triplet transition in the GS. This observation fully supports our arguments described above on the effect of exchange to lower the energy of the triplet-state in the half-filled second shell [4, 12]. Note that the second ES for $N = 4$ is also evident, and corresponds to the state $(0, -1)$ in the F–D diagram.

9.4 Electronic properties of elliptical quantum dots

9.4.1 Deformed dots in rectangular mesa devices

For a rectangular mesa, the lateral confining potential of the dot is expected to be elliptical-like due to rounding at the corners provided the number of electrons in the dot is not too large, or too small [7, 14]. Assuming the confining potential is still perfectly parabolic, we choose to characterize the 'ellipticity' by a deformation parameter, $\delta = E_\mathrm{S}/E_\mathrm{L}$. Here, $E_\mathrm{S}(E_\mathrm{L})$ is the confinement energy at 0 T along the minor (major) axis ($E_\mathrm{S} > E_\mathrm{L}$) as indicated in figure 9.2. The 2D states in the elliptical dot are labelled by the quantum numbers $(n_\mathrm{L}, n_\mathrm{S})$, where

$n_{\mathrm{L}}(n_{\mathrm{S}})$ is a quantum number $(= 0, 1, 2, \ldots)$ associated with the energy parabola along the major (minor) axis [5]. The energy of single-particle state $(n_{\mathrm{L}}, n_{\mathrm{S}})$ is $(n_{\mathrm{L}} + 1/2)E_{\mathrm{L}} + (n_{\mathrm{S}} + 1/2)E_{\mathrm{S}}$.

For a perfectly circular mesa, we trivially generalize our definition of δ so that $\delta = \beta = 1$. On the other hand, for the rectangular mesas, there is no simple correspondence between β, a ratio of lengths characteristic of the top metal contact, and δ, a ratio of energies characteristic of the dot in the mesa, and is dependent on V_{g} (or equivalently N). This means 'accidental' degeneracies will he hard to see over an extended range of N, and in any case may be lifted if the confinement potential is not completely parabolic. Nevertheless, although we are not saying that $\delta = \beta$, we assume that β is a 'measure' of δ, and thus one expects $\delta_Z > \delta_Y > \delta_X > \delta_W$.

Figure 9.4 shows the B-field evolution up to 6 T of the first 10 single-particle energy levels for a circular dot ($\delta = 1$) and elliptical dots ($\delta = 1.5, 2, 3.2$) calculated according to the model described by Madhav and Chakraborty [5] with a fixed confinement energy of $E_{\mathrm{Q}} = 3$ meV. The confinement energies for the elliptical dots are simply derived from the relation $E_{\mathrm{L}}E_{\mathrm{S}} = E_{\mathrm{Q}}E_{\mathrm{Q}}$. For the circle and the $\delta = 3.2$ ellipse, quantum numbers (n, ℓ) and $(n_{\mathrm{L}}, n_{\mathrm{S}})$, respectively, for some of the states are indicated.

As the deformation is gradually increased, figures 9.4(*a*)–(*d*), degeneracies of the single-particle states at 0 T are generally lifted, although accidental degeneracies can occur at certain 'magic' deformations, for example, (*b*) and (*c*), leading to subshell closures, provided the confining potential remains perfectly parabolic. The resulting patterns, however, are very different from that for the circular case, (*a*), and in practice may be hard to observe.

A weak B-field parallel to the current can also induce level degeneracies in both circular and elliptical dots when single-particle levels cross, but any shell structure at finite field is of a lower order and less apparent than that for the circle at 0 T [5]. As discussed before, 'wiggles' in the position of pairs of current peaks are expected at low field because of these crossings. The first lowest energy 'wiggle' originates from the crossing marked by ▲ in figure 9.4, and this crossing moves to higher energy (N) with increasing δ. The spectra also highlight other simple points (a) the B-field lifts all degeneracies present at 0 T; (b) a B-field can always induce degeneracies at finite field when single-particle levels cross, provided the confinement potential is perfectly parabolic; and (c) as δ increases, the single-particle energy level spacing generally decreases ($\leq E_{\mathrm{L}}$).

While illustrative, ultimately any modelling of real dots must go beyond a system of non-interacting electrons confined by a 2D harmonic potential, and include Coulomb interactions. Numerical diagonalization has been successfully employed to calculate basic electronic properties of dots with anisotropic confining potentials [6]. Such 'exact' calculations, however, are limited to $N \leq 6$. In order to study dots containing a larger number of electrons, spin-density functional theory is a powerful technique, which explicitly incorporates the electron–spin interactions, and has led to a number of interesting predictions

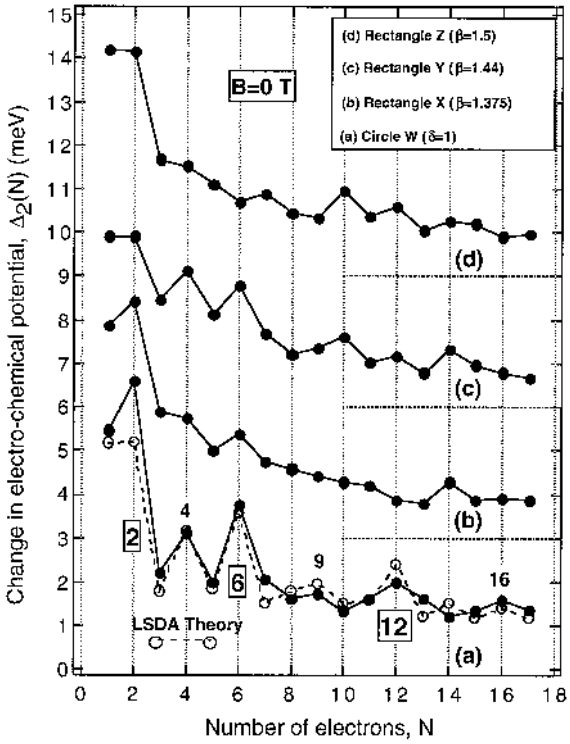

Figure 9.7. $\Delta_2(N)$, for the circular mesa W, (*a*) and the three rectangular mesas X, Y, and Z, (*b*)–(*d*) [7, 14]. The traces are offset vertically by 3 meV for clarity. The fit for W is given by a local spin-density approximation (LSDA) (see figure 9.10).

for the GS structure of dots [14, 15]. Both approaches predict changes in the addition energy spectra, and transitions in the spin-states as deformation is varied. An example of the latter is the breakdown of the conditions for which Hund's first rule gives a triplet-spin state for $N = 4$, and this is marked by a transition from a spin-triplet to a spin-singlet configuration at some critical deformation [6, 14].

We first discuss the energy spectra at 0 T measured for devices with different β-values. We measure the Coulomb oscillations, and derive the change in the electrochemical potential, $\Delta_2(N)$, for each device. The results are shown in figure 9.7 as a function of electron number, N, up to $N = 17$ for (*a*) W, (*b*) X, (*c*) Y and (*d*) Z at 0 T [7, 14]. The data for W is the same as that shown in figure 9.2. The result from a local spin-density approximation (LSDA) calculation is also included [14, 15]. The 2D shell structure including the effects of Hund's first rule is well reproduced by the calculation.

For circle W, as N is decreased, $\Delta_2(N)$ becomes generally larger due to the increase of the Coulomb interaction when a dot is 'squeezed'. This is also true for

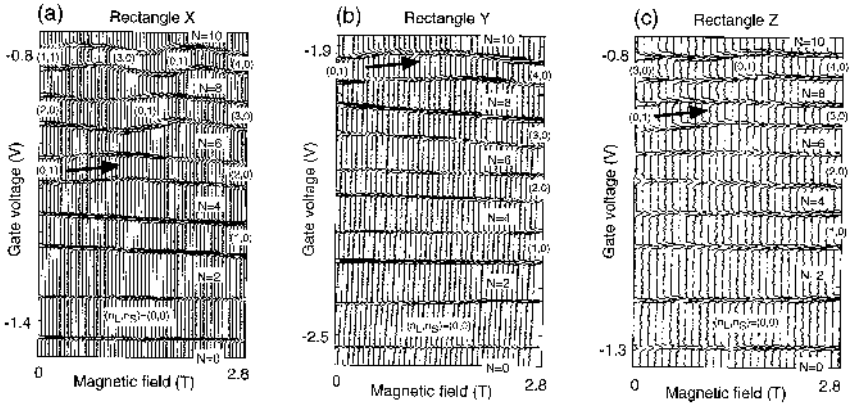

Figure 9.8. *B*-field dependence of the Coulomb oscillation peak positions for the mesas X, Y and Z, (*a*)–(*c*). The *B*-field is parallel to the current [14].

the rectangular mesas, but now there are no prominent maxima at $\Delta_2(2, 6, 12)$. The shell structure for the circular dot has now become disrupted or 'smeared out', and this is attributed directly to the lifting of the degeneracies of the single-particle states present in a circular dot [4, 7]. Deformation kills the shell structure for a circle, and even quite a small deformation can make a big difference [6, 14]. This is evident from traces, (*b*)–(*d*) in figure 9.7. The effect of deformation is discussed later in a comparison with model calculations.

9.4.2 Magnetic field dependence

Figure 9.8 shows the *B*-field dependence, for a weak field applied parallel to the current, of the Coulomb oscillation peak positions for the rectangular mesas X, Y and Z, (*a*)–(*c*) [14]. The data consists of current versus V_g traces taken at a very small bias at different *B*-fields. Peaks are paired, and there are no obvious deviations close to 0 T for $N = 4$ due to exchange effects. Quantum numbers (n_L, n_S) of the single-particle states are assigned, and the first upmoving pair of peaks is marked by a thick arrow. With increasing δ, from the calculated spectra in figure 9.4, both the first up-moving pair of peaks, and the lowest single-particle level crossing (identified in figure 9.4 by ▲) are simply expected to move systematically to higher N (or equivalently to higher energy) [5, 14].

For the elliptical dots, normal peak pairing, even from 0 T, occurs so the spin-state for $N = 4$ is a singlet. The exchange effect is maximal for a circular dot at $N = 4$ because the $(n\ell) = (0, 1)$ and $(0, -1)$ states are degenerate at 0 T and their wavefunctions have the same symmetry, but with deformation these states become the $(n_L, n_S) = (1, 0)$ and (0,1) states in an elliptical dot, which are split at 0 T. This energy splitting, γ, increases with δ. If $\gamma < E_{EX}$ at 0 T, exchange can still operate to lower the energy, and thus the $N = 4$ GS remains a spin-

triplet. On the other hand, if $\gamma > E_{\mathrm{EX}}$ at 0 T, the energy gain due to exchange is not sufficiently large to compensate for the splitting, so normal pairing occurs. Thus, we can expect a triplet–singlet transition at some critical deformation. The absence of deviations to the normal peak pairing at $N = 4$ in figures 9.8(*a*)–(*c*) apparently confirms that δ is greater than 1.2–1.3 in line with calculations we present shortly (see figure 9.10) [6, 14].

A striking feature about figures 9.8(*a*)–(*c*) is the position of the first up-moving pair of peaks. For X, Y, and Z respectively, it is the third, fifth and fourth pair of peaks. As revealed by figure 9.4, in a simple single-particle picture, the first up-moving state is $(n_{\mathrm{L}}, n_{\mathrm{S}}) = (0, 1)$ [5, 14]. Inspection of these spectra shows that this state is, in the weak-field limit, from the bottom, the third, fourth, and fifth state respectively for $1 \leq \delta < 2$, $2 \leq \delta < 3$, $3 \leq \delta < 4$. Thus, starting from $\delta = 1$, the first up-moving pair of peaks should go from the third to fourth, fourth to the fifth, ... at certain 'magic' deformations as δ is increased. Given that Coulomb effects are neglected in this simple picture, and that in practice δ is expected to vary with N, it looks as if $1 < \delta < 2$ for X, $3 < \delta < 4$ for Y, $2 < \delta < 3$ for Z. Although ellipses X, Y, and Z are deformed beyond the triplet–singlet transition, we must conclude the following: (a) δ can be much higher than that suggested by the β values; and (b) the ordering given by increasing β values may not always reflect the true ordering in δ, i.e. deformation in Y seems to be stronger than in Z, so the true sequence may be W–X–Z–Y for the four mesas. The former is not so unexpected since we have no independent way of measuring δ, but the latter is perhaps more surprising.

9.4.3 Study of Zeeman effect on the spin states

From studying the addition energy spectra of the rectangular mesa devices, we find that in the presence of an asymmetric lateral confinement, the shell structure is readily disrupted, and that a spin singlet is favoured for the $N = 4$ GS at 0 T. However, neither the addition energy spectra, nor the B-field dependence of Coulomb oscillation peaks give *direct* information about the spin states, or whether the state is a singlet or triplet. For example, at $N = 4$ the change of the electrochemical is large both for the circular mesa W and rectangular mesa Y, although the $N = 4$ GS is a triplet for the former (in line with Hund's first rule), and is a singlet for the latter, as deduced *indirectly* by applying a B-field parallel to the current. To see the effect of deformation on the spin state we measure the Zeeman effect by applying a B-field perpendicular to current [16]. The electrochemical potential for the N-electron GS $\mu(N)$, decreases or increases with B-field, depending on whether the *change* of the total spin is positive or negative, respectively, on addition of an extra electron to the $N - 1$-electron GS. The B-field dependence of $\mu(N)$ is given by,

$$\mu(N, B) - \mu(N, B = 0\ \mathrm{T})(\equiv \Delta\mu_N(B)) = g(S_N - S_{N-1})\mu_{\mathrm{B}}B, \qquad (9.3)$$

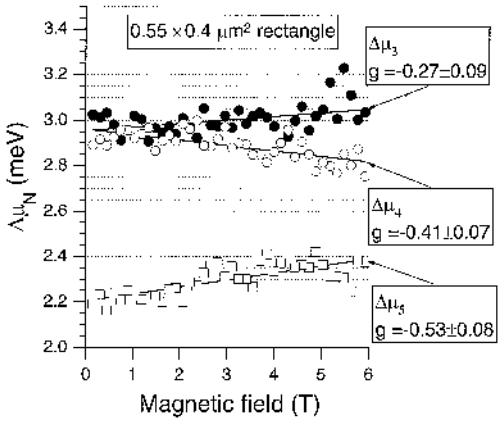

Figure 9.9. Zeeman shift of the levels, μ (3), μ(4) and μ (5), for the elliptical dot in the 0.55×0.4 μm rectangular mesa (X) [16]. The straight lines are fits to the data, which are used to estimate the electronic g-factor.

where g is the electronic g-factor, and S_N is the total spin of the N-electron GS. Let us now consider the case of $N = 4$. When the GS of the half-filled second shell is a spin-singlet, $\Delta\mu_N(B)$ is given by,

$$\Delta\mu_3(B) = \Delta\mu_3(0) - g\mu_B B,$$
$$\Delta\mu_4(B) = \Delta\mu_4(0) - g\mu_B B,$$

and

$$\Delta\mu_5(B) = \Delta\mu_5(0) - g\mu_B B. \tag{9.4}$$

On the other hand, when the $N = 4$ spin state is a triplet,

$$\Delta\mu_3(B) = \Delta\mu_3(0),$$
$$\Delta\mu_4(B) = \Delta\mu_4(0) - g\mu_B B,$$

and

$$\Delta\mu_5(B) = \Delta\mu_5(0). \tag{9.5}$$

Note that a plot of $\Delta\mu_N(B)$ versus B is useful as we can also correct for the influence of background charge on the Coulomb oscillation peaks which sometimes causes the peaks to drift a little during the course of the measurement.

Figure 9.9 shows the B-field dependence of $\Delta\mu_N$ measured for $N = 3$, 4, and 5 for the elliptical dot in mesa X (0.55×0.4 μm^2) [16]. The B-field up to 6 T is applied perpendicular to current. $\Delta\mu_3$ and $\Delta\mu_5$ increase with B-field, and $\Delta\mu_4$ decreases. The increase of $\Delta\mu_3$ with B-field indicates that the third and fourth electrons to enter the dot have opposite spins, i.e. the spin-state is a singlet. The decrease of $\Delta\mu_4$, and increase of $\Delta\mu_5$ indicate that the fifth and

sixth electrons also enter spin-up, and spin-down respectively into the next state. As a consequence, we attribute the relatively large $\Delta_2(4)$ for the elliptical dots (see figure 9.7(*b*)–(*d*)) to the lifting of the degeneracy of the single-particle states originally present in the circular dot. In figure 9.9, we estimate the electron g-factor by fitting a straight line to the data. The estimated g-factor ranges from -0.27 to -0.54, and this is comparable to the value for bulk $In_xGa_{1-x}As$ for small x [17].

9.5 Comparison to model calculations

We apply the methods of spin-density functional theory (SDFT) to model the changes to the shell structure due to the deformation of dot's lateral confinement at 0 T. To obtain the GS energies and densities for N electrons confined in an externally imposed potential, we solve the spin-dependent single-particle Kohn–Sham (KS) equations [18],

$$\left[-\frac{\hbar^2}{2m^*}\nabla_r^2 + V_{\text{eff}}^{\sigma}(r)\varphi_{i,\sigma}(r) -\right] = \varepsilon_{i,\sigma}\varphi_{i,\sigma}(r), \tag{9.6}$$

in a plane-wavebasis to avoid any symmetry restrictions. In equation 9.6, the index σ accounts for the spin ($\uparrow$ or $\downarrow$), and $\boldsymbol{r} = (x, y)$. The effective mean-field potential, $V_{\text{eff}}^{\sigma}(r)$, contains contributions from the external harmonic confining potential, the Hartree potential of the electrons, and the functional derivative of the local exchange-correlation energy, for which we use the approximation of Tanatar and Ceperley [19] (see also [15, 20] for details). The electrostatic confinement due to the lateral depletion region imposed by the side wall and the Schottky gate is approximated by a 2D anisotropic harmonic potential with frequencies $\omega_x = \omega\sqrt{\delta}$ and $\omega_y = \omega/\sqrt{\delta}$,

$$V_{\text{ext}}(x, y) = \frac{1}{2}m^*\omega^2\left(\delta x^2 + \frac{1}{\delta}y^2\right). \tag{9.7}$$

The ratio of the oscillator frequencies, $\delta = \omega_x/\omega_y$, thus defines the ratio of the major and minor axes of the ellipsoidal equipotentials. We impose the constraint, $\omega^2 = \omega_x\omega_y$, which is equivalent to conserving the area of the quantum dot with deformation [20]. The x- and y-axes are indicated in figure 9.2. With this convention, the above-defined E_{S} and E_{L}, respectively, correspond to $\hbar\omega_x$ and $\hbar\omega_y$. The strength, ω, of the external parabolic confinement leading to an average particle density, $n_0 = 1/(\pi r_{\text{s}}^2)$, in a circular dot is approximated by $\omega^2 = e^2/(4\pi\varepsilon_0\varepsilon m^* r_{\text{s}}^3\sqrt{N})$ [15]. Minimizing the energy density functional by self-consistently solving the above KS equations, GS energies are obtained for different electron numbers and deformation parameters. Full technical details are given elsewhere [15, 20], and here we report only the results. We emphasize that from recent measurements, it is clear that as N increases the confinement weakens

in such a way that the particle density tends to a constant [21]. This is implicit in our model, as for any given value of r_s, the oscillator frequency ω, and the related frequencies ω_x and ω_y, decrease with increasing N. δ is also kept constant for simplicity, although δ is expected to vary with N in practice.

There are no fitting parameters in the equations, and only a suitable choice of r_s is required to generate the addition energy spectra. The value of $r_s = 1.5a_B^*$ used in the model calculations is realistic as the value estimated experimentally for a circular quantum dot is 1.3 to $1.4a_B^*$ [21]. $a_B^* = \hbar^2(4\pi\varepsilon_0\varepsilon)/m^*e^2$ is an effective atomic unit, which for GaAs is about 10.3 nm. $r_s = 1.5a_B^*$ in the model presented here corresponds to an effective confinement energy, E_Q, for $N = 1$ of about 5.7 meV. This value is consistent with the upper limit of E_Q observed in practice (about 5 meV [12]), and justifies the $E_Q = 3$ meV value as a reasonable average for calculating the simple single-particle spectra shown in figure 9.4 for the first 10 levels.

Figure 9.10 shows $\Delta_2(N)$, calculated for quantum dots with various values of δ [14]. The lowest trace is the calculation for the circular dot, and reproduces well the familiar shell structure for a 2D harmonic oscillator. The agreement with experiment is strikingly good (see also figure 9.7(*a*)). Deforming the confinement slightly by changing the deformation parameter to $\delta = 1.1$ (trace (b) in figure 9.10), the calculation still predicts fairly clear shell closures at $N = 2$, 6 and 12. These numbers can still be considered as 'magic', but the actual values of $\Delta_2(2, 6, 12)$ are noticeably suppressed, because degeneracies have been lifted [7, 14]. As the deformation increases further, the peaks for $N = 2$, 6, 12, and 20 are further suppressed. This is a simple consequence of the removal of the level 'bunching' with deformation. Even for the cases where 'accidental' subshell closures occur at certain 'magic' deformations, for example, $\delta = 1.5$, and 2 as seen in figure 9.4, the reduced separation between degenerate single-particle energy levels (E_L) would make any shell structure less clear to observe, and the sequence of 'magic' numbers would be very different (e.g. for $\delta = 2$ it would be 2, 4, 8, 12, 18, ...) compared to those for $\delta = 1$.

Also apparent is that a systematic detailed one-to-one correspondence of $\Delta_2(N)$ between traces (*b*)–(*d*) in figure 9.7 and traces (*b*)–(*f*) in figure 9.10 is impossible to make. Although the experimental data for mesa X partly resembles the theoretical data for $\delta = 1.1$ to 1.3, the data for mesas Y and Z do not seem to resemble that for $\delta > 1.3$, except perhaps for a weak tendency to oscillate between even-N and odd-N.

Theoretically, figure 9.10 shows that there are transitions in the GS spin-configurations with deformation [20]. The total spin, S, is identified by different symbols in the figure. These transitions are particularly numerous for, but are not restricted to, the even-N systems, and are clearly very sensitive to the actual value of the deformation. For example, in the case of $N = 6$, the total spin is predicted to change from $S = 0$ (i.e. a paramagnetic state) at $\delta = 1$, through an $S = 0$ spin-density wave (SDW) state [15, 20], to $S = 1$ at $\delta = 1.5$: an indication of 'piezo-magnetic' behaviour [20, 22], i.e. changes of the dot magnetization with

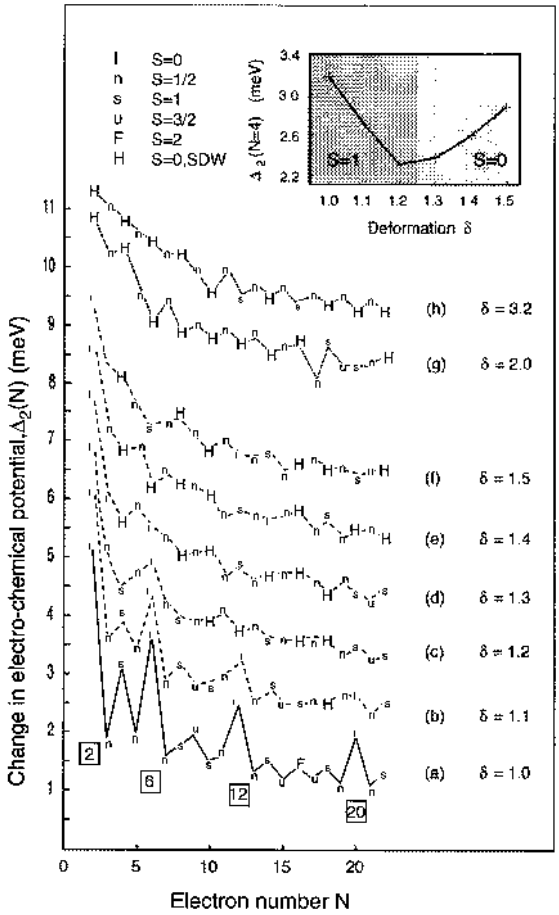

Figure 9.10. Model calculations for the change in electrochemical potential within spin-density functional theory [14]. The different traces correspond to zero, weak and moderate deformation parameters $\delta = 1.0$ to 1.5, (*a*)–(*f*), and higher deformation parameters $\delta = 2$ and $\delta = 3.2$, (*g*) and (*h*). The traces are offset vertically by 1 meV for clarity, and there is an additional 1 meV offset between traces (*f*) and (*g*). The total spin, *S*, for different deformations and electron numbers are identified by different symbols as defined in the figure. The inset shows $\Delta_2(N = 4)$ versus δ.

deformation. Although experimentally we are not in a position to differentiate between an $S = 0$ 'normal' state and an $S = 0$ SDW state with broken spin symmetry in the internal coordinates [23]—indeed the interpretation of a SDW is still debated in the literature [24]—the SDFT calculations described here predict that the latter becomes more prevalent for even-N systems as δ increases,

particularly for small average particle densities [15, 20].

Another interesting case is what happens to the $N = 4$ GS. The inset in figure 9.10 shows $\Delta_2(N = 4)$ versus deformation up to $\delta = 1.5$. Starting with the circular dot, Hund's first rule gives a total spin of $S = 1$ for the triplet state favouring spin alignment of the two electrons in the second shell rather than a total spin of $S = 0$ for the singlet state in which the spins are paired. As the deformation is initially increased, the energy separation between the two levels $(n_L, n_S) = (1, 0)$ and $(0, 1)$—the two originally degenerate levels $(n\ell) = (0, 1)$ and $(0, -1)$ in the second shell of the circular dot—increases (see (a) and (b) in figure 9.4), and so the spin-triplet state becomes progressively less favourable. $\Delta_2(4)$ continuously decreases with δ, and at a value between 1.2 and 1.3, a spin-zero state (actually predicted by the SDFT described here to be a SDW) appears. For higher values of δ, $\Delta_2(4)$ starts to increase. Other recent calculations employing numerical diagonalization for elliptical dots have also revealed a spin triplet–singlet transition at about $\delta = 1.2$ for $N = 4$ [6].

Inspection of figure 9.7 gives values of $\Delta_2(4)$ for mesas W, X, Y, and Z respectively of 3.1, 2.7, 3.1, and 2.5 meV. Whilst it is reassuring that these energies lie in the range predicted by SDFT, it is tempting to say that the trend for mesas W, X, and Y is consistent with that predicted in figure 9.10, i.e. $N = 4$ is a spin-triplet for W, and a spin-singlet for X, and Y, *and* attribute the apparently anomalously low value for Z to sample specific fluctuations [4].

For mesas Y and Z, the $\Delta_2(N)$ traces in figure 9.7 seem to show a weak tendency to oscillate between a slightly larger even-N value, and a slightly smaller odd-N value, and this oscillation seems clearer for Y than for Z. For the moment we do not try to account for the clarity of this oscillation in dots Y and Z, but try to explain the origin of the oscillation, although we are now being forced to entertain the idea that δ for Y and Z may be much larger than 1.5. Starting from the over simple single-particle picture with a fixed confinement energy, and then including a constant interaction which is the same for even-N and odd-N, a larger even-N value is expected, because only Δ_2 (even-N) can contain a finite contribution due to the single-particle energy level spacing. A slightly more advanced model, which is more realistic in principle, would be to have a constant interaction for odd-N (electron added to an $S = 1/2$ state already containing one electron) that is stronger than the constant interaction for even-N (electron added to an empty state). If the former is larger than the latter plus the single-particle spacing (more likely in practice as N increases), a weak tendency to oscillate between smaller even-N and larger odd-N could occur. This pattern is what the SDFT calculations predict in figure 9.10 for $\delta = 2$ and $\delta = 3.2$. The fact that $\Delta_2(N)$ for Y and Z is often a little larger for even-N than odd-N should not be taken to mean that the constant interaction model is more accurate. Rather the Coulomb interactions may not be so strong in practice, due to screening by the leads for example, as those in our model—and model that also does not include the self-consistent calculation of the electrostatic confining potential. Indeed, in the SDFT calculations of Lee *et al* [25], the electrostatic confining potential is much stronger

(e.g. $E_S = 20$ meV, $E_L = 10$ meV), and they find that $\Delta_2(N)$ is generally a little larger for even-N than for odd-N.

9.6 Conclusions

We have experimentally and theoretically investigated the electronic properties of circular and ellipsoidally deformed quantum dots containing a few electrons. Associated with the cylindrical symmetry and the parabolicity of the lateral confinement potential, atom-like properties such as a clear shell structure, and filling in accordance with Hund's first rule are all observed at zero-magnetic field for the circular dot. These atom-like features, as identified in the addition energy spectrum, are readily disrupted in the elliptical dots even for a small anistropy breaking circular symmetry. Application of a magnetic field parallel to the current leads to a systematic modification of the energy spectrum for the circular dot, reflecting the Fock–Darwin diagram and normal antiparallel spin filling of the same orbital states. At zero-magnetic field, parallel spin filling is only favoured in line with Hund's first rule when each shell is half-filled. For the second shell, this is well identified from measurement of excitation spectra, i.e. the $N = 4$ ground state is a spin-triplet. In contrast, for the elliptical dots, the $N = 4$ ground state is a spin-singlet due to the lifting of the single-particle level degeneracies. This spin-singlet is confirmed by measuring the Zeeman effect in an elliptical dot. These observations on the effects of deformation are in good agreement with recent theories, as well demonstrated here by the application of spin-density functional theory at zero-magnetic field. Interestingly, this theory predicts the existence of $S = 0$ SDW states in strongly deformed dots. This has not yet been clarified in the present set of experiments, although the magnetic field dependence strongly suggests that the anisotropy of an elliptical dot can be significantly higher than that expected from the geometry of the mesa in which the dot is located. To investigate the possible existence of SDW states, *in situ* manipulation of the lateral potential geometry of a quantum dot is highly desirable, and this may be achieved by fully exploiting a multiple-gated vertical single electron transistor we have recently developed [26].

Acknowledgments

We would like to acknowledge T Honda, R van der Hage, J Janssen, T Oosterkamp, H Tamura, Y Tokura and T Uesugi for their help and useful discussions. This work is partly supported by the Specially Promoted Research, grant-in-aid for scientific research from the Ministry of Education, Science and Culture in Japan, the NEDO joint research program (NTDP-98), the Dutch Organization for Fundamental Research on Matter (FOM) and the Academy of Finland, and the TMR program of the European Community under contract ERBFMBICT972405.

References

[1] For reviews, Altshuler B L, Lee P A and Webb R A (ed) 1991 *Mesoscopic Phenomena in Solids* (Amsterdam: Elsevier)
Meirav U and Foxman E B 1996 *Semicond. Sci. Technol.* **11** 255
Sohn L L, Kouwenhoven L P and Schoen G (ed) 1997 *Proc. NATO Advance Study Institute on Mesoscopic Electron Transport (Kluwer Series E345)* (Dordrecht: Kluwer)

[2] Reed M 1993 *Sci. Am.* **268** 118
Kastner M A 1993 *Phys. Today* **46** 24
Ashoori R C 1996 *Nature* **379** 413

[3] Austing D G, Honda T and Tarucha S 1996 *Semicond. Sci. Technol.* **11** 388

[4] Tarucha S, Austing D G, Honda T, van der Hage R J and Kouwenhoven L P 1996 *Phys. Rev. Lett.* **77** 3613

[5] Madhav A V and Chakraborty T 1994 *Phys. Rev.* B **49** 8163

[6] Ezaki T, Sugimoto Y, Mori N and Hamaguchi C 1998 *Semicond. Sci. Technol.* **13** A1

[7] Tarucha S, Austing D G, Honda T, van der Hage R J and Kouwenhoven L P 1997 *Japan. J. Appl. Phys.* **36** 3917

[8] Alonso M and Finn E J 1968 *Quantum and Statistical Physics* (Reading, MA: Addison-Wesley)

[9] Fock V 1928 *Z. Phys.* **47** 446
Darwin C G 1930 *Proc. Camb. Phil. Soc.* **27** 86

[10] McEuen P L, Foxman E B, Kinaret J, Meirav U, Kastner M A, Wingreen N S and Wind S J 1992 *Phys. Rev.* B **45** 11 419
McEuen P L, Wingreen N S, Foxman E B, Kinaret J, Meirav U, Kastner M A, Meier Y and Wind S J 1993 *Physica* B **189** 70
For our disk-shaped dot see Ausing D G, Tokura Y, Honda T, Tarucha S, Danoesastro M, Janssen J, Oosterkamp T H and Kouwenhoven L P 1999 *Japan. J. Appl. Phys.* **38** 372

[11] First proposal is given by Wagner M, Merkt U, Chaplik A V 1992 *Phys. Rev.* B **45** 1951
For experimental evidence see Su B, Goldman V J and Cunningham J E 1992 *Phys. Rev.* B **46** 7644
Ashoori R C, Stormer H L, Weiner J S, Pfeiffer L N, Baldwin K W and West K W 1993 *Phys. Rev. Lett.* **71** 613

[12] Kouwenhoven L P, Oosterkamp T H, Danoesastro M W S, Eto M, Austing D G, Honda T and Tarucha S 1997 *Science* **278** 1788

[13] MacDonald A H 1993 *Aust. J. Phys.* **46** 345
For our disk-shaped dot see Oosterkamp T H, Janssen J W, Kouwenhoven L P, Austing D G, Honda T and Tarucha S 1999 *Phys. Rev. Lett.* **82** 2931

[14] Austing D G, Sasaki S, Tarucha S, Reimann S M, Koskinen M and Manninen M 1999 *Phys. Rev.* B submitted

[15] Koskinen M, Manninen M and Reimann S M 1997 *Phys. Rev. Lett.* **79** 1389

[16] Sasaki S, Austing D G and Tarucha S 1998 *Physica* B **256–258** 157

[17] Wimbauer Th., Oettinger K, Efros Al. L, Meyer B K and Brugger H 1994 *Phys. Rev.* B **50** 8889

[18] Kohn W and Sham L J 1965 *Phys. Rev.* **140** A1133

[19] Tanatar B and Ceperley D M 1989 *Phys. Rev.* B **39** 5005

[20] Reimann S M, Koskinen M, Kolehmainen J, Manninen M, Austing D G and Tarucha S 1999 *Eur. J. Phys.* D to appear
[21] Austing D G, Tokura Y, Honda T, Tarucha S, Danoesastro M, Janssen J, Oosterkamp T H and Kouwenhoven L P 1999 *Japan. J. Appl. Phys.* **38** 372
[22] Reimann S M, Koskinen M and Manninen M 1999 *Phys. Rev.* B **59** 1613
[23] Ring P and Schuck P 1980 *The Nuclear Many-Body Problem* (New York: Springer)
[24] Hirose K and Wingreen N S 1999 *Phys. Rev.* B **59** 4604
[25] Lee I-H, Rao V, Martin R M and Leburton J-P 1998 *Phys. Rev.* B **57** 9035
[26] Austing D G, Honda T and Tarucha S 1998 *Physica* E **2** 583
Austing D G, Honda T and Tarucha S 1997 *Semicond. Sci. Technol.* **12** 631